Investigating the Performance of Nano Composite Membrane Pebax/TiO_2 Nanoparticle Modified with Amino Silane in the Separation of CO_2 /CH_4

Parvizi, Mohammad Reza; Saadati, Zohreh*+; Maleki, Afsaneh

Department of Chemistry, Omidiyeh Branch, Islamic Azad University, Omidiyeh, I.R. IRAN

ABSTRACT: *In the current study, an in-depth examination was conducted to evaluate how the particle size of titanium dioxide (TiO_2) will affect the mechanical, thermal, and morphological properties of the modified Pebax/TiO_2 nanoparticle membrane. TiO_2 nanoparticles were initially modified with amino silane and then incorporated into the nanocomposite Pebax/TiO_2 membrane. The obtained membranes were characterized by FT-IR, SEM, TEM, TGA, and XRD to assess the effect of modification. The result of membrane performance evaluation indicated that the solubility of the gas molecules increased within the polymer matrix when an increase in CO_2 permeability was observed. To test the performance of the nanocomposite membrane in the high-pressure separation process, the feed pressure was increased from 2 to 10 bar and the results demonstrated that the CO_2/CH_4 selectivity boosted from 16.05 to 97.74, respectively. Furthermore, when the surface of TiO_2 nanoparticles was modified by amino silane and its concentration increased in the polymer matrix, the CO_2 permeability of the nanocomposite membrane increased from 87.12 to 24.71 compared to that of the pure Pebax membrane. Experimental data were correlated with ANN (artificial neural network. The ANN of the model applied in this study includes the Levenberg-Marquardt algorithm, purelin or a linear transfer function at the output layer, and tansig or a tangent sigmoid transfer function in the hidden layer with 5 neurons.*

KEYWORDS: *CO_2/CH_4 Selectivity; Permeability; Pebax/TiO_2 nanoparticle; Amino silane nanocomposite; Separation.*

INTRODUCTION

Over the past decade, separation methods like chemical adsorption and cryogenic distillation as well as novel technologies like membrane process have gained popularity [1-4]. Moreover, industries are seeking novel methods to tackle environmental pollution, tackle energy consumption, and costs [5]. The matter of gas separation in many industrial applications is of significant importance [1, 6-10]. Besides, it requires lower operating and maintenance costs, much more user-friendly, and has the least impact on the ecosystem as well [11-14]. In comparison to conventional available separation technologies, membrane-based gas separation offers numerous advantages including, occupying a relatively smaller footprint, cost-effective, process flexibility, and high energy efficiency [15, 16]. Even though inorganic

** To whom correspondence should be addressed.*
+ E-mail: saadati.z@iauo.ac.ir
1021-9986/2023/3/754-771 18/$/6.08

membranes provide excellent gas separation performance along with high thermal and chemical stability, [17] they suffer from some challenges such as brittleness, high fabrication cost, nonscalability, and control over pore size. In contrary, polymeric membranes are attractive choices for separation applications owing to energy-effectiveness, low cost, and outstanding processability, and simplicity, and better scalability for large scale applications [18, 19].

In a study conducted by *Hassanajili et al.*, the productivity of the nanocomposite polyester membranes including metal nanoparticles was investigated for the separation of CH_4 and CO_2 pure gases. Based on their result, the gas permeability improved by increasing silica content, attributed to the increased free volume of the polymer network [20]. Such a similar trend was reported for several studies assessing the performance of polysulfone (PSF) Mixed Matrix Membranes (MMMs) with mesoporous silica MCM-41 for gas separation due to the excellent compatibility of the mesoporous materials with the polymer matrix which in turn improves the permeability of the PSF MMMs without sacrificing selectivity. Meanwhile, amine functionalized SBA-15 was reported to increase the CO_2/CH_4 selectivity in a study conducted by *Shimizu et al.* [21]. The addition of TiO_2 nanoparticles to poly (1-trimethylsilyl-1-propyne) (PTMSP) was investigated by *Matteucci et al.* and the findings revealed that the permeability CH_4 ,N_2 and CO_2 enhanced four times compared to that of the pure polymer [22]. In another research, they investigated the impact of TiO_2 nanoparticles on 1, 2-polybutadiene (PB) and the TiO_2 incorporated nanoparticles membrane demonstrated three times bigger permeability coefficients for CO_2, CH_4, N_2 and H_2 gases compared to that of the pure membrane, owing to the solubility coefficient of the gases [23]. Exploiting statistical modeling, the effect of diverse variables on the structural properties of the membranes was evaluated by incorporating Zinc oxide (ZnO), aluminum oxide (Al_2O_3), and titanium dioxide (TiO_2)nanoparticles to PMP membrane [24]. The embedment of inorganic nanomaterials into the polymers hold a special place in research due to their simplicity, mild operating conditions and stable performance [25]. Among various nanomaterials, TiO_2 nanoparticles is popular for its availability, photocatalytic activity, self-cleaning quality, ease of preparation and affordability [26]. However, the formation of TiO_2 agglomerates due to the high surface energy at higher concentrations is a negative defect and its proper dispersion is a challenge [27]. Therefore, chemical or mechanical modification of TiO_2 nanoparticles will address this challenge. Silane coupling agents seems to be the most appropriate material for adjusting its surface properties [28], decreasing the agglomeration tendency and improving the compatibility with the polymer matrix [29]. This eventually lead to appropriate chemical or physical interactions with the polymer matrix [30].

Here, TiO_2 nanoparticles were initially modified with amino silane and then different content of modified TiO_2 nanoparticle (0.5 and 1 wt.%) were incorporated into the Pebax matix, forming Pebax/TiO_2 nanocomposite membrane. The permeability, selectivity, and adsorption mechanism of the pure Pebax and Pebax/TiO_2 nanocomposite membranes were studied in detail for CO_2/CH_4 gas separation. After incorporation of the modified TiO_2 nanoparticles the CO_2/CH_4 selectivity and permeability of Pebax/TiO_2 nanocomposite membrane enhanced remarkably. Moreover, sorption studies, SEM, and tensile strength measurements were used to characterize the structure and properties of the pure and Pebax/TiO_2 nanocomposite membranes.

EXPERIMENTAL SECTION

Materials

All chemicals and solvents including Estyrene, Propane diol, Toluene and n-Hexane were purchased from Merck and Aldrich Chemical Co. and were used without further purifications. TiO_2 nanoparticles with average particle size of 25–30 nm were purchased from Nanosabz Co. (Tehran, Iran) were dried at 500 °C for almost 5 h before utilizing to evaporated any possible humidity. T3-aminopropyltriethoxysilane (APTES) was also purchased used from Merck Chemical Co. and used as the coupling agent .

Identification and evaluation devices

The morphology of samples were analyzed with Transmitting Scanning Microscopy (TEM, JEOL) and scanning electron microscopy (SEM, KYKY-EM3200, Hitachi Company, China) under an acceleration voltage of 26 kV. Fourier transform infrared spectroscopy (FT-IR, Nicolet Co, USA) was used to study the functional groups on the surface of TiO_2 nanoparticles modified with amino silane. The tensile test of nanocomposite membranes

was conducted based on the ASTM-D3039 standards with the aid of Instron (6025K) at room temperature on specimens 150 mm long, 25 mm wide and 3 mm thick, with a machine speed of 5 mm / min. Correspondingly, the of flexural strength of membrane samples was measured according to ASTM-D790 standard, using Instron (6025K) on specimens 90 mm long, 10 mm wide and 3 mm thick.

Synthesis of Pebax/TiO$_2$ nanocomposite membrane incorporated with amino silane modified TiO$_2$ nanoparticles

The casting solution of membrane was prepared by adding specific amount of Pebox (gr) to the THF solvent and the solution was stirred for 3 hours to form a homogeneous mixture. To attain such a solution, a two-step process was adopted; (i) 0.1 g of Pebax was dissolved in 2 mL THF and (ii) different quantities of m-TiO$_2$ NPs (m-TiO$_2$ nanoparticles, 0, 5, 10 and 15 wt%) were separately dispersed in 2 mL THF solution, under constant stirring for 24 h and at 25 °C. Then, two solutions were mixed to obtain the desired weight percentages of m-TiO$_2$ from 0.5 to 1.5 wt.%, Subsequently, the obtained mixture of nanocomposite Pebax/TiO$_2$ membrane nanoparticle solutions were stirred for 24h at 25°C. Afterwards, the mixture was subjected to ultrasonic ice bath for 2 h, with frequency of 2.259×10^4 Hz and power of 100 W. The solution was transferred into the glass petri dishes for solvent evaporation at ambient temperature. The final nanocomposite Pebax/TiO$_2$ membranes modified with amino silane were collected after 1 day when solvent is completely evaorized [31].

Measurement and calculation method

The permeability of CO_2/CH_4 in the nanocomposite Pebax/TiO$_2$ membranes nanoparticle modified with amino silane were calculated by a constant pressure method (a soap bubble discharge gauge). The trial entailed a gas seepage cell in which one side was exposed to the membrane and the other side was in contact with the gas feed. By making use of a regulator, the pressure on the feed side was initially adjusted and then measured by a barometer. The following equation was used to determine the gas permeability of the membranes [32]:

$$\frac{P_i}{l} = \frac{1}{A\Delta P}\frac{dv_i}{dt} \quad (1)$$

Whereby, *Pi* is the permeability of gas i, vi is the volume of gas discharged into soap bubble discharge or volume of gas permeability into the membrane in cubic centimeters, A is effective membrane surface area in square centimeter, t refers to bubble motion in column in seconds and ΔP shows the pressure drop across the membrane in centimeters of mercury. In case of GPU calculation, reports on the asymmetric membranes developed from the permeability division of the membrane thickness are available. Besides, the optimal selectivity of the two gases can be calculated via using the following equation:

$$\alpha_{i/j} = \frac{\left(\frac{P_i}{l}\right)}{\left(\frac{P_j}{l}\right)} \quad (2)$$

Where $\alpha_{i/j}$ is the optimal selectivity of gas i over j, *Pi/l* is the gas i permeability, and *Pj /l* is the gas j permeability.

Basically, it is generally accepted that the gas transfer properties of the organic/inorganic matrix membranes are hugely dependent on the membrane structure. The membrane structure is essentially dependent on the surface area and affinity between the particles and the polymer. Binomial absorption theory expresses the gas permeability in glassy polymers [33]. This theory introduces the total concentration of permeants (C) in the glassy polymer as a function of pressure (p), as follow:

$$C = k_D p + C'_H bp\ /(1 + bp) \quad (2)$$

Where K_D stands for the dissolution coefficient of artistic law and C'_H shows the cavity saturation constant. Moreover, b is the cavity continuity constant and demonstrates the ratio of the rate of constancy of absorption and desorption in the cavities. Taking into consideration that high porosity provides a place for the interaction between gases and the polymer network, the higher the porosity the higher the permeability and hence solubility.

Investigation the performance of membranes in terms of permeability and selectivity

Pressure-volume-constant-variable method can be utilized to verify the permeability prosperities of carbon dioxide and methane gases through polymeric membranes. Taking into account the steady-state conditions, the polymeric membranes developed in this method were initially pressurized for a specific duration of time

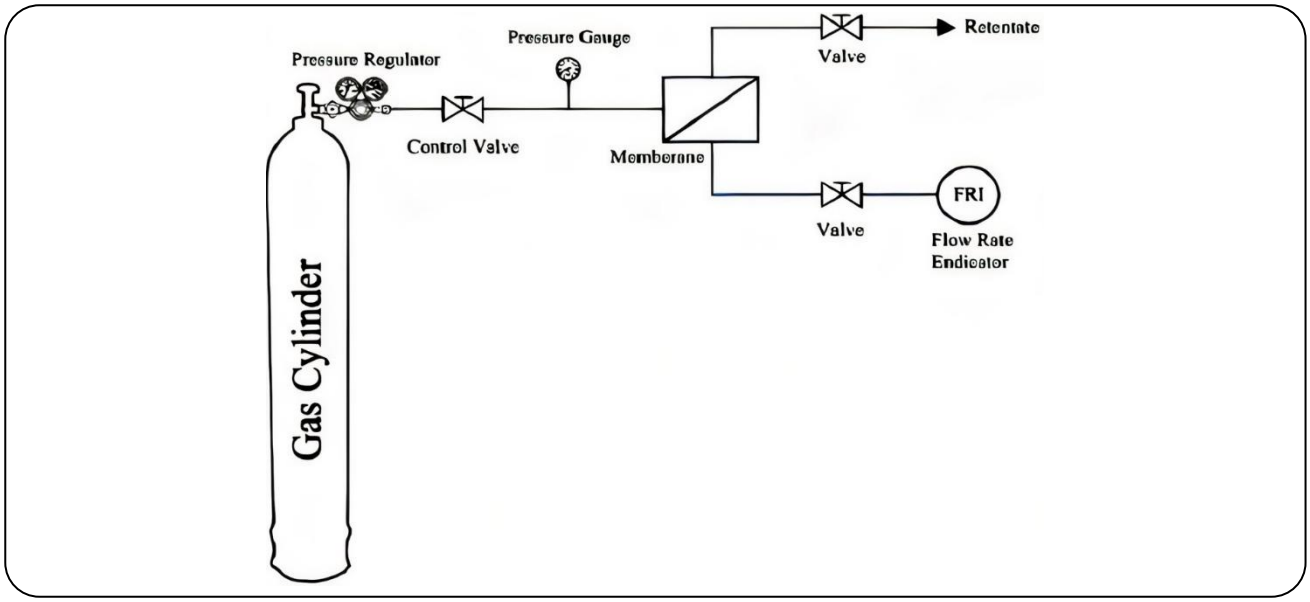

Fig. 1: Schematic permeability gas of the mixed matrix membranes.

and the volume flow rate through the membranes was recorded by a digital flow meter. The effective surface area of all membranes was estimated to be 56/71 cm^2. Every single permeability measurment was done at standard pressure and temperature. The polymeric membrane was fixed in the membrane tubes and then sealed by a hollow circular rubber ring. A gas feed inlet and two outlet portions were embedded in the membrane tube. From the two outlets, one was considered for the gas component leaked through the membrane and the other for the residual gas component. Fig. 1 represents the schematic of the apparatus applied to measure the leakage of carbon dioxide and methane from the polymeric membrane.

Artificial neural network

From the field of Artificial Neural Network model (ANN), back propagation algorithm as the training algorithm for a feed forward network has been applied. Initially, the model tried to compare the ultimate computed data for FFBP with the experimentally detected outcomes. After computation of the errors, they were used for adjusting each neuron weight. The evaluation of input variables including the CO_2/CH_4 selectivity and permeability, nanocomposite Pebax/TiO_2 membrane containing TiO_2 nanoparticle modified with amino silane, and pressure were performed all over the process. Subsequently, five neurons at 37 experimental points were employed to feed the model. Data adjustment was obtained by training, test, and validation sets contained 50%, 25% and 25% data points, respectively. Due to the application of tan-sigmoidal transfer function all of the data points were normalized in the range of [0.1, 0.9] based on the ensuing Eq. (4) as follow [34]:

$$X_{norm} = \frac{X - X_{min}}{X_{max} - X_{min}} \quad (4)$$

By assuming X as a variable in the above formula, Xmin and Xmax are is the minimum and the maximum values respectively.

RESULTS AND DISCUSSION

Characterization techniques

Examination of TiO_2 Surface Modification Process

Fig. 2 represents the FT-IR spectra of both unmodified and modified TiO_2 nanoparticles. Fig.2.a refers to the FT-IR spectrum of unmodified TiO_2 nanoparticles components while Fig. 2.b. represents that of the modified TiO_2 nanoparticles with amino-propyl triethoxy silane coupling agent. The peaks appeared around 1300 cm^{-1} and 1320 cm^{-1} can be contributed to the doublet from the asymmetric O=S=O stretching vibration and 1240 cm^{-1} to the asymmetric C–O–C stretching vibration of the aryl ether group of the PES support layer, respectively [35-37]. The peaks observed at 1120 cm^{-1} can be corresponded to the C-O-C symmetric vibration of ether group present in the PEO soft segment of the neat Pebax membrane [38, 39]. Two more peaks observed at about 1634 and 1744 cm^{-1}

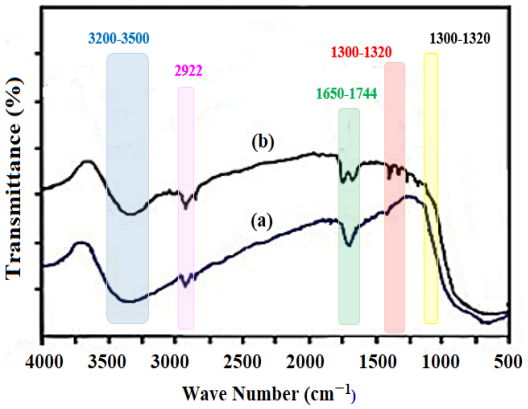

Fig. 2: (a) FT-IR spectra of the unmodified and (b) FT-IR spectra of the modified TiO_2 amino-propyl triethoxy silane.

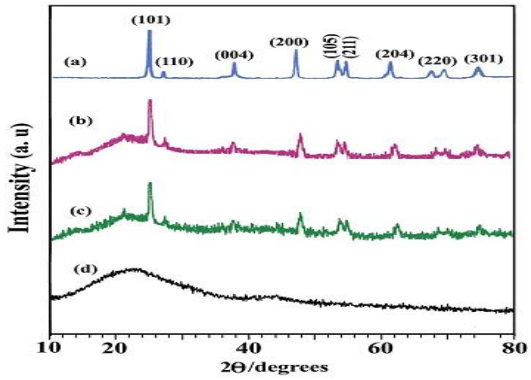

Fig. 3. XRD patterns of the surface modified TiO_2 (a), nanocomposite membranes with 0.5% (b) and 1.0% (c) of modified TiO_2 with amino silane and pure aromatic UP (d).

can be referred to of the carbonyl groups the existing in the H-N-C=O and O-C=O segment of the PA part, respectively [40]. Moreover, the aliphatic -C-H band is identified at about 2922 cm^{-1} [41]. The broad band appeared at 3398 cm^{-1} can be correspond to the stretching vibration of ─OH functions on TiO_2 NPs surface [42].

X-ray diffraction

The XRD patterns of UP, m-TiO_2 and UP with 0.5% and 1.0% of m-TiO_2 NPs are illustrated in Fig. 3. For pure UP (Fig. 3.d), it is apparent that there was a lack of diffraction signal in the range of 2θ angle barring one crystalline signal, suggesting the presence of a little proportion of crystalline phase. Since Pebax is a semi-crystalline polymer, XRD pattern of the neat membrane shows a week diffraction peak due to the amorphous region and a strong diffraction peak owing to crystalline region of the polymer matrix. The peaks around 21° and 24° of 2θ can be contributed to the rigid segment while the small peaks at 2θ about 38-41° can be related to the crystalline phase of the soft segment in Pebax [45,46]. For m-TiO_2 NPs (Fig. 3a), the apparent signals at 101, 110, 004, 200, 105, 211, 204, 220, 301 prove the presence of rutile phase which is a good evidence of the crystalline form of this compound [27]. The change in the crystallinity of Pebax can prove the intermolecular interaction between TiO_2 NPs and Pebax matrix [47]. Additionally, the characteristic signals of m-TiO_2 and UP in the XRD patterns reveal that the preparation process and surface modification cannot change the morphology of NPs (Fig.3b and c). Following the Debye-Scherrer formula, the average size of the TiO_2 nanoparticles was estimated to be about 25–35 nm.

Morphology characterization of m-TiO_2 and UP/m-TiO_2 NCs

FE-SEM and TEM analysis were used to scrutinize the microstructures and nanofiller distribution within the NCs. The FE-SEM and TEM images of the m-TiO_2 with two distinct magnifications are displayed in Fig. 4 and 5. As clearly can be seen, the nanoscale size and globular shape of the m-TiO_2 NPs has been shown in the images. Furthermore, the sizes of partic les were estimated to be in the range of 25–35 nm.

Thermal properties

ThermoGravimetric Analysis (TGA) TGA was conducted to assess the thermal decomposition temperature and weight loss of the of the modifed-TiO_2, UP/m-TiO_2 NCs and pure UP under analysis. The thermal degradation behavior of the pure TiO_2 and Pebax/TiO_2 nanocomposite membrane is measured under nitrogen atmosphere and the results is illustrated in Fig. 6. As clearly be seen, silane surface modified TiO_2 NPs showed lower thermal stability compared to that of the pure one. The slight weight loss of unmodified TiO_2 NPs (roughly 2%) over the whole temperature ranges of 0–800°C could be ascribed to the elimination of water and partial dehydroxylation of the TiO_2 NPs. Based on TGA curve presented in Fig. 6b, the of m-TiO_2 demonstrated an evident two-step decomposition route, the former mass

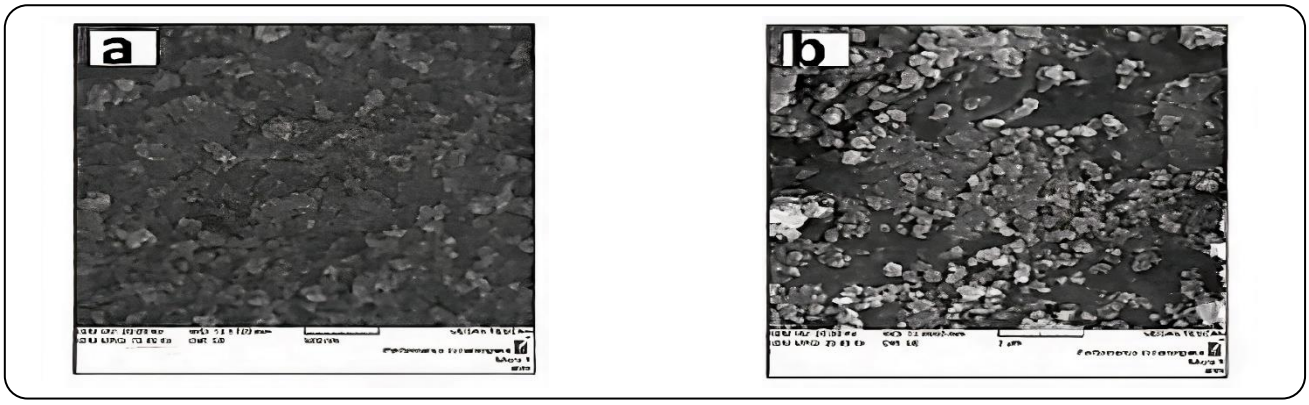

Fig. 4: (a, b) FE-SEM images of surface modified TiO_2 nanoparticles at different magnifications.

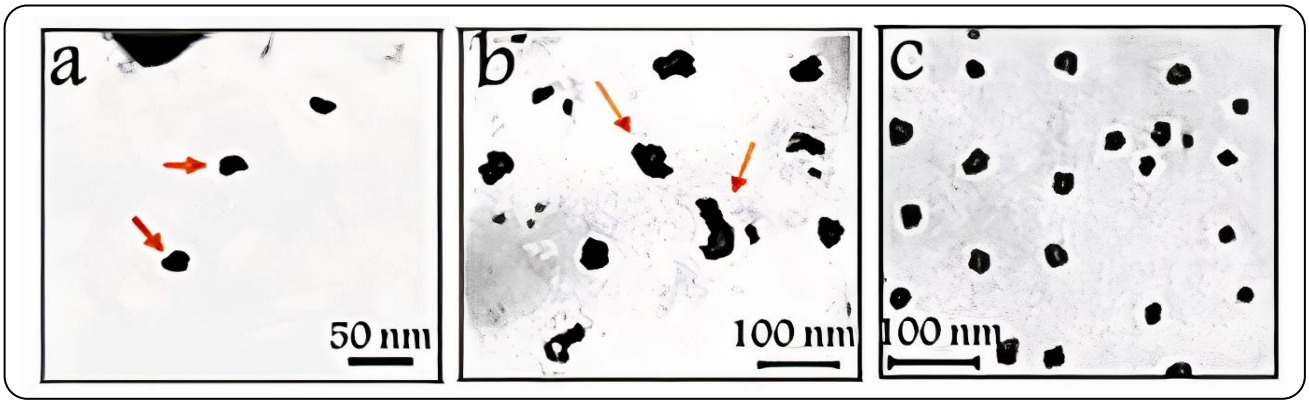

Fig. 5: (a, b, c) TEM images of surface modified TiO_2 nanoparticles at different magnifications.

loss occurs in the temperature ranges of 150-250 °C while the latter one observed at 450–550 °C. The first one could be attributed to the presence of hydroxide functional group on the surface of the TiO_2 NPs. Moreover, the TGA curves of the UP and UP/m-TiO_2 nanocomposite membranes are presented in Fig. 7 whereby a weight loss is observed by temperature increment. The gradual weight loss of the membranes can be ascribed to the decomposition of the polymer and the evaporation of entrapped solvent. To conduct a close examination of thermal stability, the TGA and weight loss of the UP/m-TiO_2 nanocomposite membranes containing 0.5 and 1.0 wt.% ($T_{0.5}$ and $T_{1.0}$) of m-TiO_2 NPs were measured over the temperature range of 0-800 ˚C (char yield). In parallel, as summarized in Table 1, the concentration of m-TiO_2 concentration in polymer matrix has a direct relation with the thermal stability. In other words, when higher concentration of m-TiO_2 is loaded into the polymer matrix, an increment of thermal stability will be observed owing to the formation of highly cross-linked network structures. The primary reason behind such a finding can be attributed to the presence of m-TiO_2 nanoparticles which act as thermal insulator and also form a mass transport barrier to the volatile products produced during decomposition of the nanocomposite membrane. Besides, since the char yield is of prime importance for estimating the LOI Limiting Oxygen Index (LOI) values, the LOI was carried out for the UP/m-TiO_2 NCs over the range of 43–46%. Considering the definition, the Limiting Oxygen Index (LOI) is the minimum percentage of oxygen required for the combustion of materials and its value enhances with char yield increment, as stated by *Van Krevelen* [43]. Therefore, based on this explanation, nanocomposite membranes could be classified as the self-quenching materials.

LOI = 17.5 + 0.4CR, Where CR = char yield.

Based on the estimation of LOI values carried out for UP/m-TiO_2 NCs in range of 43–46%, the NCs could be classified as the self-quenching materials.

Table 1: Thermal characterizations of the pure UP and nanocomposite Pebax/TiO_2 membrane containing different concentration of silane surface modified TiO_2 (UP/m-TiO_2 NCs).

Entry	Material	T_5 (ºC)	T_{10} (ºC)	Char yield (%)	LOI (%)
1	Pure UP	397	437	59	41.7
2	UP/m-TiO2 NC0.5%	453	476	64	43.1
3	UP/m-TiO2 NC1.0%	496	512	69	45.1

[a] *Temperature at which 0.5 and 1.0 % weight loss was recorded by TGA at a heating rate of 20°C/min in a nitrogen atmosphere.*
[b] *Percentage weight of material left undecomposed after TGA analysis at maximum temperature of 800°C in a nitrogen atmosphere.*

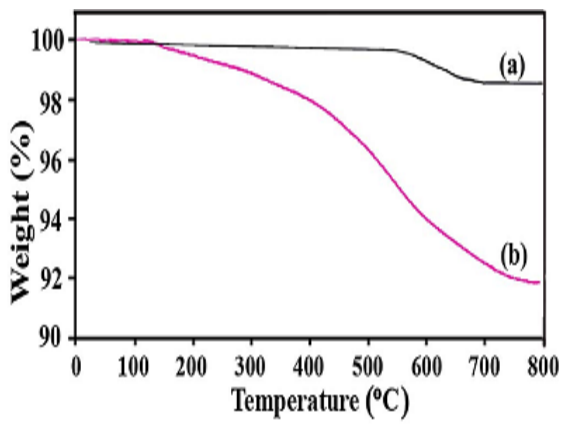

Fig. 6: TGA thermograms of pristine TiO_2 (a) and nanocomposite Pebax/ TiO_2 membrane containing modified TiO_2 (b).

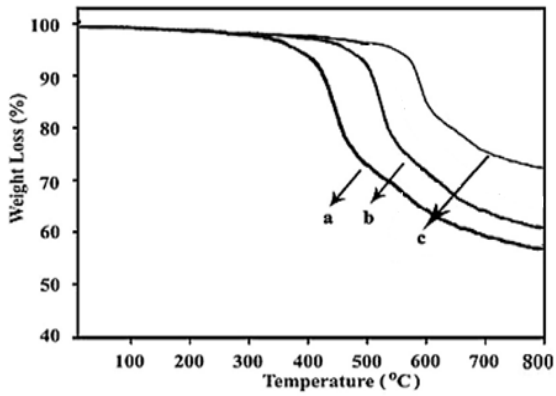

Fig. 7: TGA Thermograms of pristine UP (a), nanocomposite Pebax/TiO_2 membrane containing 0.5% (b), and 1.0% (c) silane surface modified TiO_2.

Physicomechanical properties of nanocomposite membranes

3.2.1. Morphology of prepared membranes

The SEM surface images of pure Pebax membrane showed filamentous fibers, while Pebax nanocomposite membrane containing amino silane modified TiO_2 nanoparticles presented multiple delaminated sheets on the surface. Considering the morphological properties, it can be said that a major transformation occurred from fibrous to pseudo-flowering from for the Pure Pebax and Pebax/m-TiO_2 nanocomposite membranes, respectively. Meanwhile, further evaluation on the surface changes of the pure and nanocomposite membranes proves that the apparent layers hardened the polymer-particle interface and an indistinct separation was also observed after modification [44].

Stretch test

The results of tensile strength nanocomposite membranes samples containing different concentrations of TiO_2 are presented in Fig 9-11; those of the elongation to break of the samples in the tensile test are demonstrated. As displayed in Fig. 9, with each weight of the filler phase, the tensile strength of the pristine and nanocomposite membranes increases with the concentrations of TiO_2. In case of the nanocomposite membranes incorporated with m-TiO_2, higher tensile strength was observed compared to that of the unmodified TiO_2 NPs over the all concentration range tested in this study. Both nanocomposite membranes reinforced with unmodified and modified TiO_2 nanoparticles were analyzed. However, it should be pointed out that at the same weight percent, the nanocomposite reinforced with m-TiO_2 nanoparticles showed the greater tensile strength possibly because of higher interaction between nanoparticles and the polymer phase in the nanocomposite reinforced TiO_2 nanoparticles [45, 46]. Since TiO_2 nanoparticle were initially modified with amino silane and then incorporated to the Pebax matrix, the surface of the TiO_2 nanoparticle is covered with amine-functional groups. The amine terminals result in improved compatibility of TiO_2 inorganic nanoparticles

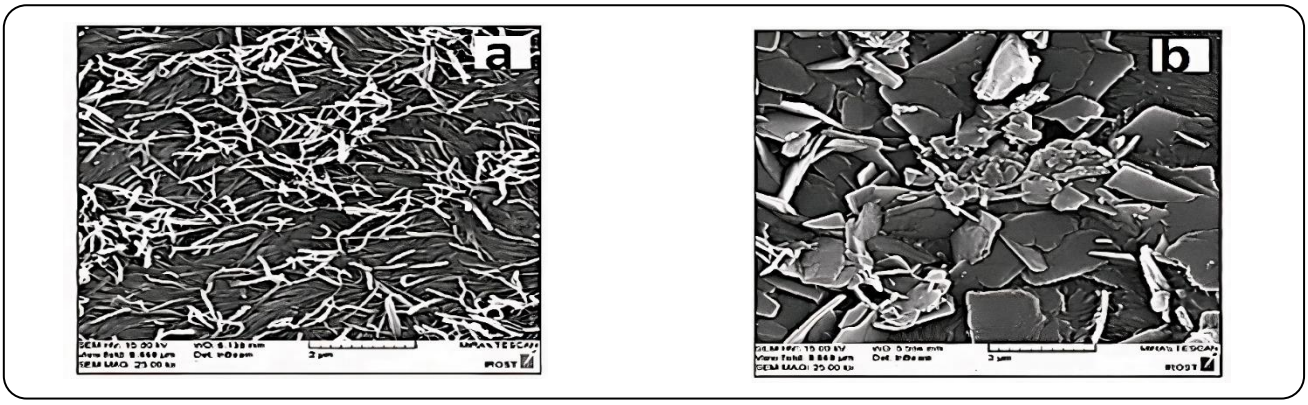

Fig. 8: SEM images of Membrane Surface (a) Pure Pebax Membrane and (b) nanocomposite Pebax/m-TiO_2 membrane Pebax Membrane.

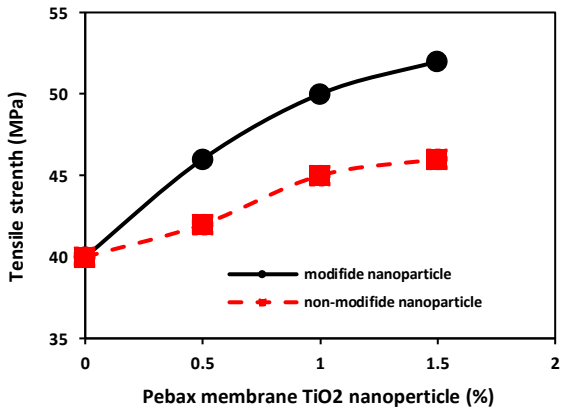

Fig. 9: Tensile strength of nanocomposite membranes containing different percentages and types of TiO_2 nanoparticles.

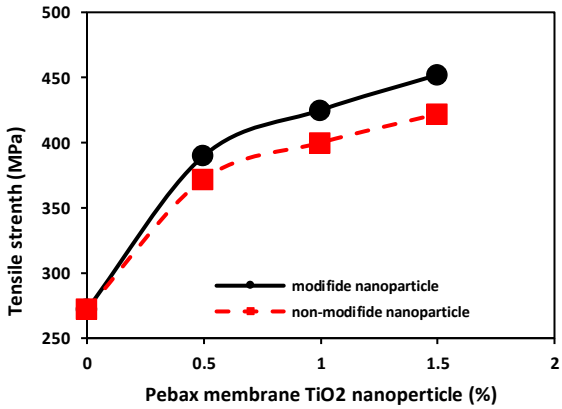

Fig. 10: Tensile models of nanocomposite membranes containing different percentages and types of TiO_2 nanoparticles.

with the Pebax polymeric chains and then increased dispersion occurs between two phases that in turn increases the elongation, tensile module, and flexibility of the final nanocomposite membranes [47]. Similar findings to were observed for the tensile modulus curve as represented in Fig. 10. However, as evident in Fig .11, the elongation at break decreased with the concentration of TiO_2 NPs and the amount of this reduction was more evident in case of nanocomposite membranes reinforced with m-TiO_2 NPs.

Bending test

The results of bending test of all the membrane samples are shown in Fig. 12. In both cases of nanocomposite membranes incorporated with modified and unmodified TiO_2 NPs, the flexural strength improved with increasing the concentration of TiO_2 NPs. Greater flexural strength was spotted for the nanocomposite membranes reinforced with m-TiO_2 NPs at the same weight percentages over all concentration ranges. This finding can be attributed to the presence of silane functional groups on the surface of m-TiO_2 ad it improves the affinity between metallic NPs and polymeric Pebax matrix. The higher the affinity ot two phases, the more uniform the dispersion of NPs whithin the nanocomposite matrix and hence higher flexural strength was eventually observed.

Impact Test Results

Studying the dependence of on two factors:

It is generally accepted that the behavior of nanocomposite materials is dependent on two main factors namely NPs size, their interaction with the matrix phase and therefore distribution within the polymeric matrix. These factors are key prerequisite to achieve desired behavior [48]. The results of bending test of the membrane samples are displayed in Fig. 13. As evident, any rise

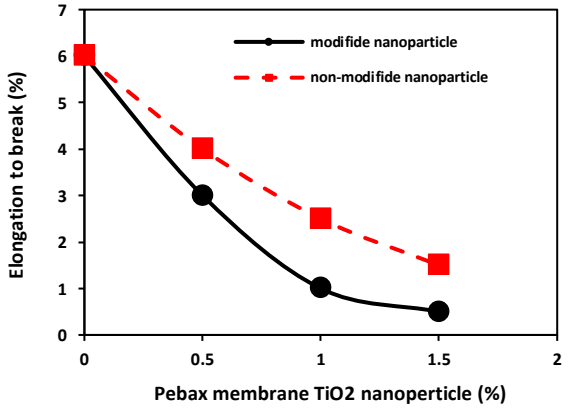

Fig. 11: The elongation to break of nanocomposite membranes containing different percentages and types of TiO_2 nanoparticles.

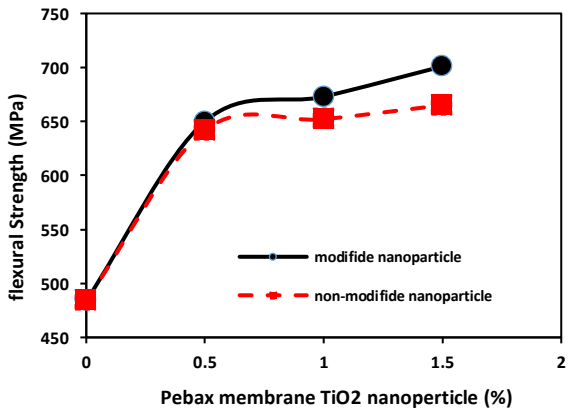

Fig. 12: The flexural strength of nanocomposite membranes containing different percentages and types of TiO_2 nanoparticles.

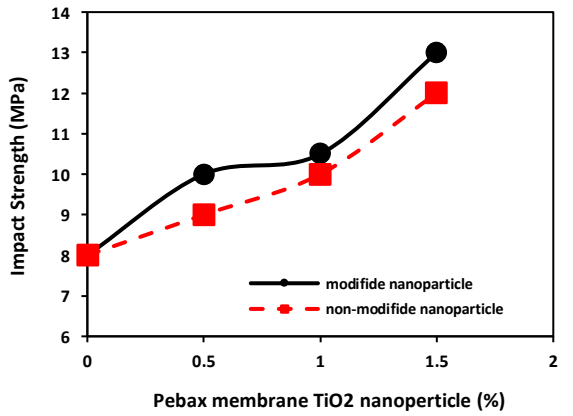

Fig. 13: The impact Strength of nanocomposite membranes containing different percentages and types of TiO_2 nanoparticles.

in the concentration of the TiO_2 NPs triggered enhanced the impact strength of both nanocomposite membranes incorporated with modified and unmodified TiO_2 NPs. However, this increase was remarkably apparent in case of m-TiO_2 NPs reinforced membranes. This behavior can be ascribed to the improved affinity and better distribution of NPs. It is belived that the presence of any agglomeration and bigger particle sizes can produce stress-focused areas and weaken the interaction between the nanoparticles and the polymer chains. Since unmodified titanium oxide NPs may result in occurring such challenges, the impact strength of the nanocomposite will finally reduce.

A thorough investigation was performed on the permeability and selectivity of carbon dioxide (CO_2) and methane (CH_4) for nanocomposite Pebax/TiO_2 membranes TiO_2 NPs modified with amino silane. The influence of these additives on the permeability of CO_2 and CH_4 in absence and presence of loading pressure are illustrated in Fig. 14 a, b. As crystal lucid, compared to that of the pristine Pebax membrane, the CO_2 permeability of nanocomposite membrane incorporated with m-TiO_2 NPs with amino silane increased with loading higher concentration of TiO_2 NPs. An enhancement from 24.71 to 87.12 was observed for the nanocomposite membrane containing 1 wt% of m-TiO_2 NPs. This increase can be corresponded to the presence of cavities due to the increase of free volume and the improved solubility of CO_2 inside the polymeric nanocomposite membranes. However, in both cases of the nanocomposite membranes containing modified and unmodified TiO_2 NPs, higher CO_2 permeability was observed compared to that of the CH_4 permeability[49]. Therefore, the recognition of the CO_2/CH_4 selectivity of is impossible (Table. 2) due to highly low value of the CO_2 permeability. However, the superior selectivity of the nanocomposite membranes as well as the unique properties of the membranes based on the Pebax copolymer can be confirmed by the results (Fig. 14 a, b).

As summarized in Table 3, some major achievements are presented for the previously reported Pebax®1657 membranes including mixed matrix or blended ones in different fabrication conditions and operating conditions applied for CO_2/CH_4 separation. In comparison to the reported Pebax®1657 membranes, our modified TiO_2 nanocomposite membrane offer improved characteristic and gas separation performance, potentially great option to use in large scale gas separation plants.

Table. 2: Separation performance for pure Pebax membranes (without TiO_2 NPs).

Pressure (bar)	Permeability (barrer)		Selectivity	membrane
	CO_2	CH_4		
4	24.71	1.54	16.05	pure Pebax membranes (without nanoparticles)
6	34.78	1.12	31.05	
8	54.97	0.928	59.23	
10	73.21	0.749	97.74	

Table 3: Summary of CO2/CH4 separation performance for several types of Pebax®1657 membranes modified with different types of additives.

Additive name	Loading (%wt.)	P (bar)	T (°C)	CO2 Permeance (GPU) (CO2 Permeability (Barrer))	CO2/CH4 selectivity	Ref.
ZIF-8-IP	8	2	30	23.10 (261)	36	[50]
NaX-COOH	15	6	25	12.52 (187.8)	57.41	[51]
f-GO	0.7	2	35	(172)	17.1	[52]
Zn-TCPP	7	2	25	5.9 (626)	65	[53]
MCN	0.5	4	25	(123)	20	[54]
MIL-53(Al)	10	10	35	(129)	23.3	[55]
NH2-MIL-53(Al)	10	10	35	(149)	20.5	[55]
UiO-66	2	7	25	14.8 (369.3)	31.3	[56]
UiO-66-NH2	1.5	7	25	15.7 (393.4)	39.8	[56]
MXene	0.1	4	25	1810	15	[18]
ZIF-8	20	3	25	(200)	15.1	[57]
ZIF-8	8	8	30	92.25 (655)	16.4	[58]
ImGO	0.8	8	25	(76.20)	30	[59]
CNF-UiO	3	6	25	13.14 (328.4)	27.4	[60]
NOTT-300	40	10	25	(395)	36.3	[61]
SiO2-COOH	8	2	25	(133)	45	[62]
TEPA-MIL-101	5	4	25	19.43 (34.6)	46.33	[63]
CMC	3.75	4	25	14.85 (51.97)	47.22	[64]
Ni-NH2-BDC	5	6	20	7.14 (31.55)	94	[47]
Pure Pebax	-	10	25	()	73.21	

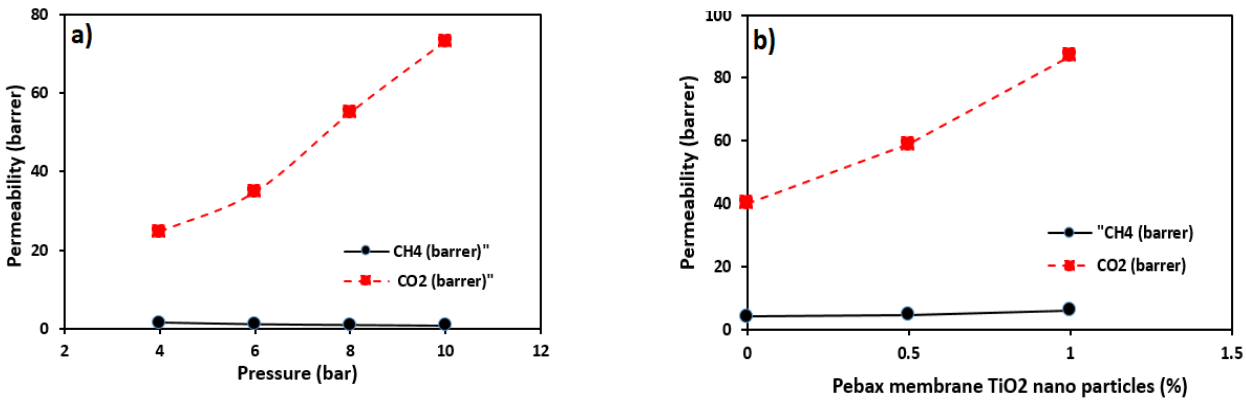

Fig. 14: The permeability of CO_2/CH_4 gases of the nanocomposite membranes containgm-TiO_2 NPs in a) absence and b) presence of applying pressure (4 bar).

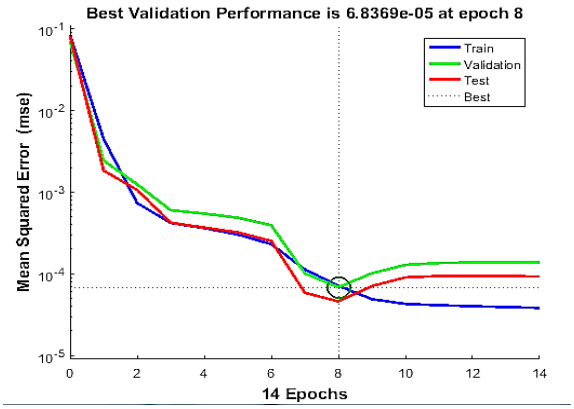

Fig. 15. Gradual change of training, validation, and test errors as a function of the number of training epochs during neural network model for CO_2 selectivity and permeability for nanocomposite Pebax/TiO_2 membrane incorporated with TiO_2NPs modified with amino silane.

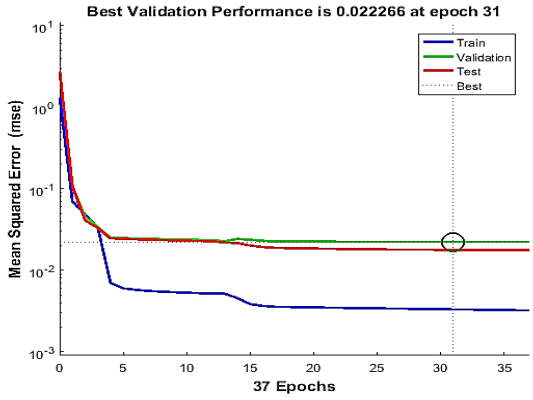

Fig. 16: Gradual change of training, validation, and test errors as a function of the number of training epochs during neural network model for CH_4 selectivity and permeability for nanocomposite Pebax/TiO_2 membrane incorporated with TiO_2NPs modified with amino silane.

Artificial Neural Network (ANN) modeling

Regarding the importance membrane-based gas separation technology, mathematical modeling provides a vital tool in the design process of the natural gas plants for CO_2 separation. The presence of reliable mathematical models for the performance prediction of the natural gas plants minimizes the technical risks [65-67]. Furthermore, it also eradicates the necessity of the time-consuming and expensive pilot plants and experimental studies to evaluate the operating conditions and membrane specification. Although the effectiveness of computational intelligence such as neural networks in engineering science has been demonstrated [68-72], few studies reported the use of ANN to evaluate the Pebax nanocomposite membrane performance. In this regard, we applied ANN analysis to validate the developed models based on the experimental data. Based on the obtained results, it was demonstrated that ANN modeling could be a good candidate for predicting the separation behavior of CO_2/CH_4 mixtures in Pebax/TiO_2 nanocomposite membrane in the absence of data from laboratory experiments. In this regard, three functions of weight (training), net input, and transfer (tansig) monitor and control the network function and performance. At epoch numbers 14, five neurons at 37 experimental points were selected. MSE (mean square error) of 0.607 in ANN model was spotted for CO_2/CH_4 selectivity and permeability. As it is evident from the plot of error histogram in Fig. 15-21, the errors are very negligible in this process. In this study, based upon the function of error performance, the MSE had the minimum value at 5 neurons during the net training process [73, 74]. The ANN model with four input layers (including initial CO_2/CH_4 concentration, nanocomposite Pebax/TiO_2 membrane TiO_2 NPs modified with amino silane, pressure and Temperature) premised on the output layers (deletion of target compounds) was proved to be significantly reliable for predicting and reckoning the CO_2/CH_4 selectivity and permeability. Table. 4, 5 clearly present the MSE and the correlation coefficients (R^2) for train, test, and validation of the CO_2/CH_4 selectivity and permeability.

The summary of the comparison of the error mean sum of squares, the mean absolute error, the standard deviation, the sum squares error, and the correlation coefficient for the findings of the model has been provided in Tables 4, 5. The results of ANN model demonstrated the relative superiority of the CO_2/CH_4 permeability of selectivity. Furthermore, the lowest permeability error clearly showed the perfect contribution of nanocomposite Pebax/TiO_2 membrane incorporated with TiO_2 NPs modified with amino silane for the permeability of CO_2/CH_4 selectivity.

CONCLUSIONS

In the current study, the TiO_2 nanoparticle were initially modified with amino silane and then the permeability of TiO_2 nanoparticles incorporated Pebax nanocomposite membrane was tested by CO_2/CH_4 gas mixture at different pressures. The findings revealed that

Table 4: Juxtaposition of 1–22 neurons in the hidden layer for CO_2/CH_4 selectivity by ANN model development with the Levenberg – Marquardt algorithm.

Standard deviation	Average	High(+1)	Low (-1)	Parameter type	Factors
2.5	5.0	10	2	InPut Network	pressure (barrer)
1.0	0.75	1.5	0.5	InPut Network	membrane Pebax/TiO_2 nanoparticle modified with amino silane nano composite (mol/L)
35	60	40	25	InPut Network	Tempreture
0.25	0.5	1.0	0.1	InPut Network	CO_2/CH_4 selectivity
25.258	32.234	89.487	4.156	OutPut Network	% metronidazole drug

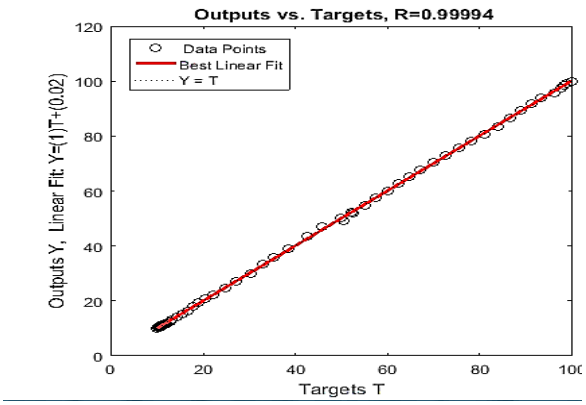

Fig. 17: Juxtaposition of Experimental (Objective) and Neural Network Outputs in Test and Total Data Stages for the CO_2 selectivity and permeability for nanocomposite Pebax/TiO_2 membrane incorporated with TiO_2NPs modified with amino silane.

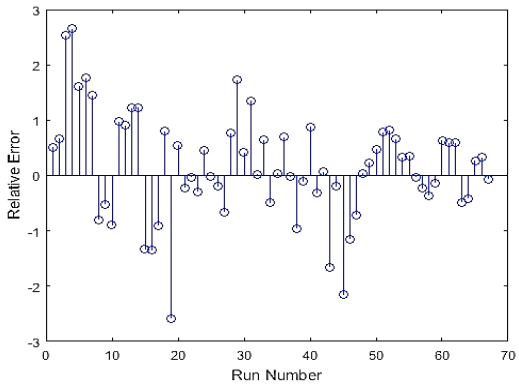

Fig. 19: The exhibition of the plot of Relative error histogram for permeability on the CO_2 selectivity for nanocomposite Pebax/TiO_2 membrane incorporated with TiO_2NPs modified with amino silane.

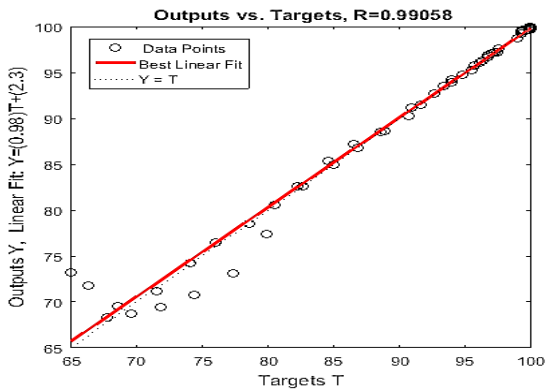

Fig. 18: Juxtaposition of experimental (objective) and neural network outputs in test and total data stages for the ch_4 selectivity and permeability for nanocomposite Pebax/TiO_2 membrane incorporated with TiO_2NPs modified with amino silane.

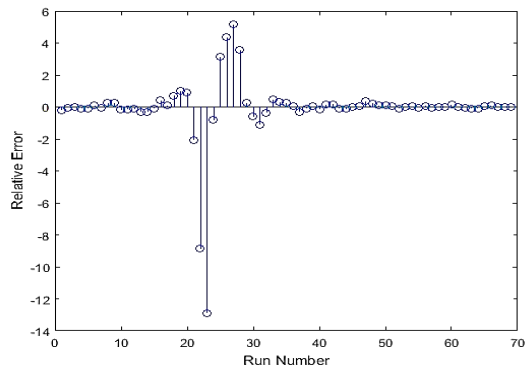

Fig. 20: The exhibition of the plot of relative error histogram for permeability on the CH_4 selectivity for nanocomposite Pebax/TiO_2 membrane incorporated with TiO_2NPs modified with amino silane.

Table 5: Statistical juxtaposition of three ANN models.

gas	SSE	MSE	AARE	SD	R^2
CO_2	12.747	0.607	0.0362	0.4893	0.99983
CH_4	10.815	0.515	0.0314	0.4539	0.99991

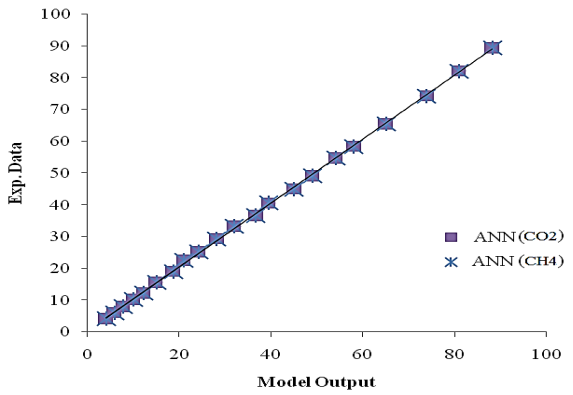

Fig. 21: The exhibition of the plot of juxtaposition of the outputs of all three models with experimental values for permeability on the CO_2/CH_4 selectivity for nanocomposite Pebax/TiO_2 membrane incorporated with TiO_2NPs modified with amino silane.

there is a direct relationship between the CO_2 permeability and the elasticity of the polymeric membrane, meaning the tensile strength can affect the CO_2 permeability at high pressures. In other words, elongation was observed for high concentrations of CO_2 absorbed onto the membrane surface, increasing the CO_2 permeability due to the improved solubility of the CO_2 molecules in the polymer matrix. Besides, there is inverse relation between CH_4 permeability and applied pressure whereby CH_4 permeability decreased by pressure increment. Additionally, the feed pressures increment resulted in improved performance and the selectivity of CO_2/CH_4 increased from 16.05 to 97.74 when the applied pressure enhanced from 2 to 10 bar. The same behavior was observed for the Pebax/TiO_2 nanocomposite membrane in which the CO_2 permeability nanocomposite membrane surged from 24.71 to 87.12 after amino silane modification. Meanwhile, such an ascending trend was also observed for CO_2/CH_4 selectivity of the nanocomposite membrane, as amino silane introduces numerous amin functional groups that have proper affinity to CO_2 polar molecules. To further assess the creditability of the results, the neural network analysis including three models was employed. Considering the permeability and CO_2/CH_4 selectivity values after amino silane incorporation, the results confirmed that the Pebax/TiO_2 nanocomposite membrane provided the lowest errors. All these findings demonstrate superior performance of the nanocomposite membranes in terms of permeability and CO_2/CH_4 selectivity.

Acknowledgments

The authors would like to acknowledge and thank the partial support of the Islamic Azad University, Omidiyeh Branch, in this work.

Received : Dec. 10, 2021 ; Accepted : June 13, 2022

REFERENCES

[1] Soleymanipour S.F., Dehaghani A.H.S., Pirouzfar V., Alihosseini A., The Morphology and Gas-Separation Performance of Membranes Comprising Multiwalled Carbon Nanotubes/Polysulfone–Kapton, *Journal of Applied Polymer Science*, **133**: 34 (2016).

[2] Heydari S., Pirouzfar V., The Influence of Synthesis Parameters on the Gas Selectivity and Permeability of Carbon Membranes: Empirical Modeling and Process Optimization Using Surface Methodology, *RSC Advances*, **17**: 14149-14163 (2016).

[3] Zeinali S., Aryaeinezhad M., Improving O_2/N_2 Selective Filtration Using Carbon Nanotube-Modified Mixed-Matrix Membranes, *Chemical Engineering & Technology*, **38**: 2079-2086 (2015).

[4] Barquın A. F., Coterillo C.C., Palomino M., Valencia S., Irabien A., Current Status And Future Prospect of Polymer-Layered Silicate Mixedmatrix Membranes for CO_2/CH_4 Separation, *Chem Eng Technol*, **38**: 658-666 (2015).

[5] Nematollahi M.H., Dehaghani A.H.S., Abedini R., CO_2/CH_4 Separation with Poly (4-methyl-1-pentyne)(TPX) Based Mixed Matrix Membrane Filled with Al_2O_3 Nanoparticles, *Korean Journal of Chemical Engineering*, **33**: 657-665 (2016).

[6] Jamshidi M., Pirouzfar V., Abedini R., Pedram M.Z., The Influence of Nanoparticles on Gas Transport Properties of Mixed Matrix Membranes: An Experimental Investigation and Modeling, *Korean Journal of Chemical Engineering*, **34**: 829-843 (2017).

[7] Khoshakhlagh A.H., Beygzadeh M., Golbabaei F., Carrasco-Marín F., Shahtaheri S.J., Optimization of Adsorption Parameters of Activated Carbon Modified with the Oxidizing Agent on Adsorptive Removal of Toluene Using Response Surface Methodology (RSM), *Journal of Dispersion Science and Technology*, **42**: 2101-2115 (2021).

[8] Khoshakhlagh A.H., Beygzadeh M., Golbabaei F., Saadati Z., Carrasco-Marín F., Shahtaheri S.J., Isotherm, Kinetic, and Thermodynamic Studies for Dynamic Adsorption of Toluene in Gas Phase onto Porous Fe-MIL-101/OAC Composite, *Environmental Science and Pollution Research*, **27**: 44022-44035 (2020).

[9] Khoshakhlagh A.H., Golbabaei F., Beygzadeh M., Carrasco-Marín F., Shahtaheri S.J., Toluene adsorption on Porous Cu–BDC@OAC Composite at Various Operating Conditions: Optimization by Response Surface Methodology, *RSC Advances*, **10**: 35582-35596 (2020).

[10] Khoshakhlagh A.H., Carrasco Marín F., Evaluation of Direct Reading Photoionization Detector Performance under Various Operational Parameters, *Environmental Health Engineering and Management Journal* , **8**: 123-128 (2021).

[11] Alihosseini A., Dadfar E., Aibod S., Synthesis and Characterization of Novel Poly (Amide- Imide) Nanocomposite/Silicate Particles Based on N-Pyromellitimido-L-Phenyl Alanine Containing Sulfone Moieties, *Journal of Applied Chemical Science International*, : 84-92 (2015).

[12] Rahmanian B., Pakizeh M., Mansoori S.A.A., Abedini R., Application of Experimental Design Approach and Artificial Neural Network (ANN) for the Determination of Potential Micellar-Enhanced Ultrafiltration Process, *Journal of Hazardous Materials*, **187**: 67-74 (2011).

[13] Kiamehr Y., Naser I., Rafizadeh M., Mohammadi A.H., Mixed Matrix Membranes Using SAPO-34/APMDES/PES for Carbon Dioxide/Methane Separation, *Iranian Journal of Chemistry and Chemical Engineering (IJCCE)*, **41(2)**: 566-581 (2020).

[14] Omrani H., Naser I., Rafiezadeh M., Preparation and Characterization of a Novel Polysulfone (PS) Mixed Matrix Membrane Modified with a SAPO-34 Nanofiller for CO_2/CH_4 Gaseous Mixture Separation, *Iranian Journal of Chemistry and Chemical Engineering (IJCCE)*, **41(3)**: 902-912 (2021).

[15] Jung H.J., Han S.H., Lee Y.M., Yeo Y.K., Modeling and Simulation of Hollow Fiber CO_2 Separation Modules, *Korean Journal of Chemical Engineering*, **28**: 1497-1504 (2011).

[16] Lock S.S.M., Lau K.K., Ahmad F., Shariff A.M., Modeling, simulation and Economic Analysis of CO_2 Capture from Natural Gas Using Cocurrent, Countercurrent and Radial Crossflow Hollow Fiber Membrane, *International Journal of Greenhouse Gas Control*, **36**: 114-134 (2015).

[17] Ghalei B., Wakimoto K., Wu C.Y., Isfahani A.P., Yamamoto T., Sakurai K., Higuchi M., Chang B.K., Kitagawa S., Sivaniah E., Rational Tuning of Zirconium Metal–Organic Framework Membranes for Hydrogen Purification, *Angewandte Chemie International Edition*, **58**: 19034-19040 (2019).

[18] Shamsabadi A.A., Isfahani A.P., Salestan S.K., Rahimpour A., Ghalei B., Sivaniah E., Soroush M., Pushing Rubbery Polymer Membranes to be Economic for CO_2 Separation: Embedment with Ti_3C_2T x MXene Nanosheets, *ACS Applied Materials & Interfaces*, **12**: 3984-3992 (2019).

[19] Low Z.X., Budd P.M., McKeown N.B., Patterson D.A., Gas Permeation Properties, Physical Aging, and its Mitigation in High Free Volume Glassy Polymers, *Chemical Reviews*, **118**: 5871-5911(2018).

[20] Hassanajili S., Masoudi E., Karimi G., Khademi M., Mixed Matrix Membranes Based on Polyetherurethane and Polyesterurethane Containing Silica Nanoparticles for Separation of CO_2/CH_4 Gases, *Separation and Purification Technology*, **116**: 1-12 (2013).

[21] Chaidou C.I., Pantoleontos G., Koutsonikolas D.E., Kaldis S.P., Sakellaropoulos G.P., Gas Separation Properties of Polyimide-Zeolite Mixed Matrix Membranes, *Separation Science and Technology*, **47**: 950-962 (2012).

[22] Moghadam F., Omidkhah M.R., Vasheghani-Farahani E., Pedram M.Z., Dorosti F., The Effect of TiO_2 Nanoparticles on Gas Transport Properties of Matrimid5218-based Mixed Matrix Membranes, *Separation and Purification Technology*, **77**: 128-136 (2011).

[23] Momeni S.M., Pakizeh M., Preparation, Characterization and Gas Permeation Study of PSf/MgO Nanocomposite Membrane, *Brazilian Journal of Chemical Engineering*, **30**: 589-597 (2013).

[24] Ahn J., Chung W.J., Pinnau I., Guiver M.D., Polysulfone/silica Nanoparticle Mixed-Matrix Membranes for Gas Separation, *Journal of Membrane Science*, **314**: 123-133 (2008).

[25] Yang Y., Zhang H., Wang P., Zheng Q., Li J., The Influence of Nano-Sized TiO_2 Fillers on the Morphologies and Properties of PSF UF Membrane, *Journal of Membrane Science*, **288**: 231-238 (2007).

[26] Mutiso R.M., Winey K.I., Electrical Properties of Polymer Nanocomposites Containing Rod-Like Nanofillers, *Progress in Polymer Science*, **40**: 63-84 (2015).

[27] Mallakpour S., Asadi P., Structural Features of Bionanocomposite Derived from Novel Designed Poly (ester-imide) Based on Natural Amino Acids with Hydroxyl Segments Tailored for Better Dispersion of TiO_2 Nanofiller, *Bulletin of Materials Science*, **36**: 203-212 (2013).

[28] Iijima M., Tsukada M., Kamiya H., Effect of Particle Size on Surface Modification of Silica Nanoparticles by Using Silane Coupling Agents and Their Dispersion Stability In Methylethylketone, *Journal of Colloid and Interface Science*, **307**: 418-424 (2007).

[29] Neouze M.A., Schubert U., Surface Modification and Functionalization of Metal and Metal Oxide Nanoparticles by Organic Ligands, *Monatshefte Für Chemie-Chemical Monthly*, **139**: 183-195 (2008).

[30] Mallakpour S., Dinari M., Neamani S., A Facile and Green Method for the Production of Novel and Potentially Biocompatible Poly (Amide-Imide)/ ZrO_2–Poly (vinyl alcohol) Nanocomposites Containing Trimellitylimido-l-Leucine Linkages, *Progress in Organic Coatings*, **86**: 11-17 (2015).

[31] Heydari M., Moheb A., Ghiaci M., Masoomi M., Effect of Cross-Linking Time on the Thermal and Mechanical Properties and Pervaporation Performance of Poly (Vinyl Alcohol) Membrane Cross-Linked with Fumaric Acid Used for Dehydration of Isopropanol, *Journal of Applied Polymer Science*, **128**: 1640-1651 (2013).

[32] Wong K.C., Goh P.S., Ismail A.F., Thin Film Nanocomposite: the Next Generation Selective Membrane for CO_2 Removal, *Journal of Materials Chemistry A*, **4**: 15726-15748 (2016).

[33] Shafie S.N.A., Liew W.X., Md Nordin N.A.H., Bilad M.R., Sazal, N., PutraZ. A., Wirzal M.D.H., CO_2-Philic [EMIM][Tf_2N] Modified Silica in Mixed Matrix Membrane for High Performance CO_2/CH_4 Separation, *Advances in Polymer Technology*, 1-11 (2019).

[34] Asfaram A., Ghaedi M., Azqhandi M.A., Goudarzi A., Dastkhoon M.J.R.A., Statistical Experimental Design, Least Squares-Support Vector Machine (LS-SVM) and Artificial Neural Network (ANN) Methods for Modeling the Facilitated Adsorption of Methylene Blue Dye, *RSC advances*, **6**: 40502-40516 (2016).

[35] Wei X., Wang Z., Wang J., Wang S., A Novel Method of Surface Modification to Polysulfone Ultrafiltration Membrane by Preadsorption of Citric Acid or Sodium Bisulfite, *Membr. Water Treat*, **3**: 35-49 (2012).

[36] Seyedpour S.F., Rahimpour A., Najafpour G., Facile in-Situ Assembly of Silver-Based MOFs to Surface Functionalization of TFC Membrane: A Novel Approach Toward Long-Lasting Biofouling Mitigation, *Journal of Membrane Science*, **573**: 257-269 (2019).

[37] Mozafari M., Seyedpour S.F., Salestan S.K., Rahimpour A., Shamsabadi A.A., Firouzjaei M.D., ... & Soroush, M. Facile Cu-BTC Surface Modification of Thin Chitosan Film Coated Polyethersulfone Membranes With Improved Antifouling Properties for Sustainable Removal of Manganese, *Journal of Membrane Science*, **588**: 117200 (2019).

[38] Kim J.H., Lee Y.M., Gas Permeation Properties of Poly (Amide-6-B-Ethylene Oxide)–Silica Hybrid Membranes, *Journal of Membrane Science*, **193**: 209-225 (2001).

[39] Choi M.C., Jung J.Y., Yeom H.S., Chang Y.W., Mechanical, Thermal, Barrier, and Rheological Properties of Poly (Ether-Block-Amide) Elastomer/Organoclay Nanocomposite Prepared by Melt Blending, *Polymer Engineering & Science*, **53**: 982-991 (2013).

[40] Wang Y., Ren J., Deng M., Ultrathin Solid Polymer Electrolyte PEI/Pebax2533/AgBF4 Composite Membrane for Propylene/Propane Separation, *Separation and Purification Technology*, **77**: 46-52 (2011).

[41] Murali R.S., Kumar K.P., Ismail A.F., Sridhar S., Nanosilica and H-Mordenite Incorporated Poly (ether-block-amide)-1657 Membranes For Gaseous Separations, *Microporous and Mesoporous Materials*, **197**: 291-298 (2014).

[42] Zhang G., Lu S., Zhang L., Meng Q., Shen C., Zhang J., Novel Polysulfone Hybrid Ultrafiltration Membrane Prepared with TiO_2-g-HEMA and its Antifouling Characteristics, *Journal of Membrane Science*, **436**: 163-173 (2013).

[43] Dinari M., Haghighi A., Surface Modification of TiO_2 Nanoparticle by Three Dimensional Silane Coupling Agent and Preparation of Polyamide/Modified-TiO_2 Nanocomposites for Removal of Cr (VI) from Aqueous Solutions, *Progress in Organic Coatings*, **110**: 24-34 (2017).

[44] Bhattacharya M., Dutta S.K., Sikder J., Mandal M.K., Computational and Experimental Study of Chromium (VI) Removal in Direct Contact Membrane Distillation, *Journal of Membrane Science*, **450**: 447-456 (2014).

[45] Mehrdad A., Noorani N., Erratum to Permeability behavior of Polyvinyl Chloride-Ionic Liquid Ionomer for CO_2/CH_4 Separation , *Separation and Purification Technology*, **245**: 116885 (2020).

[46] Zhou J., Zhao F., Wang Y., Zhang Y., Yang L., Size-Controlled Synthesis of ZnO Nanoparticles and their Photoluminescence Properties, *Journal of Luminescence*, **122**: 195-197 (2007).

[47] Mousavinejad A., Rahimpour A., Shirzad Kebria M.R., Khoshhal Salestan S., Sadrzadeh M., Tavajohi Hassan Kiadeh N., Nickel-Based Metal–Organic Frameworks to Improve the CO_2/CH_4 Separation Capability of Thin-Film Pebax Membranes, *Industrial & Engineering Chemistry Research*, **59**: 12834-12844 (2020).

[48] Kausch H. H., Michler G. H., Effect of Nanoparticle Size and Size-Distribution on Mechanical Behavior of Filled Amorphous Thermoplastic Polymers, *Journal of Applied Polymer Science*, **105**: 2577-2587 (2007).

[49] Almenningen S., Gauteplass J., Hauge L.P., Barth T., Fernø M. A., Ersland G., Measurements of CH_4 and CO_2 Relative Permeability in Hydrate-Bearing Sandstone, *Journal of Petroleum Science and Engineering*, **177**: 880-888 (2019).

[50] Jomekian A., Bazooyar B., Behbahani R.M., Mohammadi T., Kargari A., Ionic Liquid-Modified Pebax® 1657 Membrane Filled by ZIF-8 Particles for Separation of CO2 from CH4, N_2 and H_2, *Journal of Membrane Science*, **524**: 652-662 (2017).

[51] Maleh, M. S., Raisi, A., CO_2-Philic Moderate Selective Layer Mixed Matrix Membranes Containing Surface Functionalized NaX Towards Highly-Efficient CO_2 Capture, *RSC Advances*, **9**: 15542-15553 (2019).

[52] Zhang J., Xin Q., Li X., Yun M., Xu R., Wang S., Li Y., Lin L., Ding X., Ye H., Zhang Y., Mixed Matrix Membranes Comprising Aminosilane-Functionalized Graphene Oxide for Enhanced CO_2 Separation, *Journal of Membrane Science*, **570**: 343-354 (2019).

[53] Li, X., Hou, J., Guo, R., Wang, Z., Zhang, J., Constructing Unique Cross-Sectional Structured Mixed Matrix Membranes by Incorporating Ultrathin Microporous Nanosheets for Efficient CO2 Separation, *ACS Applied Materials & Interfaces*, **11**: 24618-24626 (2019).

[54] Yang X., Zheng W., Xi Y., Guan W., Yan X., Ruan X., Ma C., Dai Y., He G., Constructing low-Resistance and High-Selectivity Transport Multi-Channels in Mixed Matrix Membranes for Efficient CO_2 Separation, *Journal of Membrane Science*, **624**: 119046 (2021).

[55] Meshkat S., Kaliaguine S., Rodrigue D., Mixed Matrix Membranes Based on Amine and Non-Amine MIL-53 (Al) in Pebax® MH-1657 for CO_2 Separation, *Separation and Purification Technology*, **200:** 177-190 (2018).

[56] Mozafari M., Abedini R., Rahimpour A., Zr-MOFs-Incorporated Thin Film Nanocomposite Pebax 1657 Membranes Dip-Coated on Polymethylpentyne Layer for Efficient Separation of CO_2/CH_4, *Journal of Materials Chemistry A*, **6**: 12380-12392 (2018).

[57] Sutrisna P.D., Hou J., Li H., Zhang Y., Chen V., Improved Operational Stability of Pebax-Based Gas Separation Membranes with ZIF-8: A Comparative Study of Flat Sheet and Composite Hollow Fibre Membranes, *Journal of Membrane Science*, **524**: 266-279 (2017).

[58] Jomekian A., Behbahani R.M., Mohammadi T., Kargari A., CO_2/CH_4 Separation by High Performance co-Casted ZIF-8/Pebax 1657/PES Mixed Matrix Membrane, *Journal of Natural Gas Science and Engineering*, **31**: 562-574 (2016).

[59] Dai Y., Ruan X., Yan Z., Yang K., Yu M., Li H., Zhao W., He G., Imidazole Functionalized Graphene Oxide/PEBAX Mixed Matrix Membranes for Efficient CO_2 Capture, *Separation and Purification Technology*, **166**: 171-180 (2016).

[60] Mozafari M., Rahimpour, A., Abedini, R., Exploiting the Effects of Zirconium-Based Metal Organic Framework Decorated Carbon Nanofibers to Improve CO2/CH4 Separation Performance of Thin Film Nanocomposite Membranes, *Journal of Industrial and Engineering Chemistry*, **85**: 102-110 (2020).

[61] Habib N., Shamair Z., Tara N., Nizami A.S., Akhtar F.H., Ahmad N.M., Gilani M.A., Bilad M.R., Khan A.L., Development of Highly Permeable and Selective Mixed Matrix Membranes Based on Pebax® 1657 and NOTT-300 for CO_2 Capture, *Separation and Purification Technology*, **234**: 116101 (2020).

[62] Ghadimi A., Mohammadi T., Kasiri N., Gas Permeation, Sorption and Diffusion Through PEBA/SiO2 Nanocomposite Membranes (Chemical Surface Modification of Nanoparticles), *International Journal of Hydrogen Energy*, **40**: 9723-9732 (2015).

[63] Salestan S.K., Pirzadeh K., Rahimpour A., Abedini R., Poly (ether-block amide) Thin-Film Membranes Containing Functionalized MIL-101 MOFs for Efficient Separation of CO_2/CH_4, *Journal of Environmental Chemical Engineering*, **9**: 105820 (2021).

[64] Salestan S.K., Rahimpour A., Abedini R., Experimental and Theoretical Studies of Biopolymers on the Efficient CO_2/CH_4 Separation of Thin-Film Pebax® 1657 Membrane, *Chemical Engineering and Processing-Process Intensification*, **163**: 108366 (2021).

[65] Ahmad A. L., Lau K. K., Modeling, Simulation, and Experimental Validation for Aqueous Solutions Flowing in Nanofiltration Membrane Channel, *Industrial & Engineering Chemistry Research*, **46**: 1316-1325 (2007).

[66] Makaruk A., Harasek M., Numerical Algorithm For Modelling Multicomponent Multipermeator Systems, *Journal of Membrane Science*, **344:** 258-265 (2009).

[67] Salestan S.K., Seyedpour S.F., Rahimpour A., Shamsabadi A.A., Tiraferri A., Soroush M., Molecular Dynamics Insights Into the Structural and Water Transport Properties of a Forward Osmosis Polyamide Thin-Film Nanocomposite Membrane Modified with Graphene Quantum Dots, *Industrial & Engineering Chemistry Research*, **59**: 14447-14457 (2020).

[68] Molashahi M., Hashemipour H., Experimental Study and Artificial Neural Network Simulation of Methane Adsorption on Activated Carbon, *Korean Journal of Chemical Engineering*, **29**: 601-605 (2012).

[69] Gardner M.W., Dorling S.R., Artificial Neural Networks (The Multilayer Perceptron)—A Review of Applications in the Atmospheric Sciences, *Atmospheric Environment*, **32**: 2627-2636 (1998).

[70] Ghobadian B., Rahimi H., Nikbakht A.M., Najafi G., Yusaf T.F., Diesel Engine Performance and Exhaust Emission Analysis Using Waste Cooking Biodiesel Fuel with an Artificial Neural Network, *Renewable Energy*, **34**: 976-982 (2009).

[71] Rashidi A.M., Eivani A.R., Amadeh A., Application of Artificial Neural Networks to Predict the Grain Size of Nano-Crystalline Nickel Coatings, *Computational Materials Science*, **45(2)**: 499-504 (2009).

[72] Esfandiari K., Ghoreyshi A.A., Jahanshahi M., Using Artificial Neural Network and Ideal Adsorbed Solution Theory for Predicting the CO_2/CH_4 Selectivities of Metal–Organic Frameworks: A Comparative Study, *Industrial & Engineering Chemistry Research*, **56**: 14610-14622 (2017).

[73] Kiani, M., Bagheri, S., Karachi, N., Dil, E. A., Adsorption of Purpurin Dye from Industrial Wastewater Using Mn-Doped Fe2O4 Nanoparticles Loaded on Activated Carbon, *Desalination and Water Treatment*, **152**: 366-373 (2019).

[74] Rashidi M.M., Galanis N., Nazari F., Parsa A.B., Shamekhi L., Parametric Analysis and Optimization of Regenerative Clausius and Organic Rankine Cycles with Two Feedwater Heaters Using Artificial Bees Colony and Artificial Neural Network, *Energy*, **36**: 5728-5740 (2011).